Structures, Bonding, Infrared Spectroscopy, and Two-Electron Reduction Potentials of the Coordinated Metallopnictanes $Fe_3(CO)_9(\mu_3\text{-}EML_n)_2$ (E = P, As, Sb; ML_n = $Cr(CO)_5$, $MnCp(CO)_2$)

Boyce E. Collins, Yoshihiro Koide, Cynthia K. Schauer,* and Peter S. White

Department of Chemistry, The University of North Carolina at Chapel Hill, Chapel Hill, North Carolina 27599-3290

Received June 26, 1997[⊗]

The triiron clusters $Fe_3(CO)_9(\mu_3\text{-}EML_n)_2$ (**1-E**, ML_n = $MnCp(CO)_2$, E = P, As, Sb; **2-E**, ML_n = $Cr(CO)_5$, E = P, As, Sb) can be considered cluster analogues of organopnictane (ER_3) ligands, in which the triply bridging E ligands are coordinated to 16-electron capping metal groups, ML_n. Structural parameters, infrared CO stretching frequencies, and reduction potentials for this metallopnictane series are reported. Analysis of structural, spectroscopic, and electrochemical data reveal systematic variations as a function of the capping heteroatom and the metal fragment coordinated to the heteroatom. The covalent radius of the capping heteroatom dictates the structure of the $Fe_3(CO)_9(\mu_3\text{-}E)_2$ bonding framework, and both Fe−E and Fe−Fe distances increase linearly with increasing heteroatom covalent radius. The electronegativity of the capping heteroatom (E) influences the frequencies of the Fe_3-core carbonyl stretching modes ($\nu_{CO}(Sb) < \nu_{CO}(As) < \nu_{CO}(P)$), while the two-electron reduction potentials for the series **1** and series **2** clusters ($E_{1/2}(Sb) > E_{1/2}(As) > E_{1/2}(P)$) correlate with the covalent radius of E. Clusters with capping $Cr(CO)_5$ groups are reduced at potentials ∼400 mV more positive than the $MnCp(CO)_2$-capped analogues. On the basis of the frequencies of the CO stretching modes for the capping ML_n group and the E−ML_n distance, the metallopnictance ligands are classified as intermediate between organopnictanes and halopnictanes in terms of their net electronic impact (the sum of σ-donating and π-accepting properties). Results of Fenske−Hall molecular orbital calculations provide a qualitative description of the Fe_3−E_2 bonding as a function of heteroatom (E). Trends in Mulliken populations and a Walsh analysis suggest the Fe−E bonds are strongest for the most electronegative E, phosphorus. The Fe−Fe overlap populations are nearly constant with E, despite the increase in Fe−Fe distance attendant upon incorporation of larger heteroatoms. Two-electron reduction of the metallopnictane Fe_3-core changes the donor and acceptor characteristics of the metallopnictane ligand, as demonstrated by a structure determination for $[(PhCH_2)Me_3N]_2$(**1-P**). The Mn−P distance in $(\mathbf{1\text{-}P})^{2-}$ is 0.1 Å longer than in the neutral analogue, **1-P**. Single-crystal X-ray structure determinations for **1-As**, **1-Sb**, **2-P**, **2-As**, **2-Sb**, and $[(PhCH_2)Me_3N]_2$(**1-P**) are reported.

Introduction

The role of bridging heteroatoms in dictating the structures of dinuclear and higher nuclearity cluster complexes is well established,[1] thus the incorporation of a heteroatom, E, as a face-capping ligand on a cluster surface offers a means of inducing systematic structural changes in the cluster core. We present herein a comprehensive analysis of the periodic trends in the structures, bonding, infrared spectroscopy, and electrochemistry of the triiron bicapped $Fe_3(CO)_9(\mu_3\text{-}EML_n)_2$ clusters that result from changes in heteroatom, E = P, As, and Sb, and the capping metal group, ML_n = $MnCp(CO)_2$ and $Cr(CO)_5$. Trends in the properties of $Fe_3(CO)_9(\mu_3\text{-}EML_n)_2$ clusters are interpreted in terms of a $Fe_3(CO)_9(\mu_3\text{-}E)_2$ "ligand" coordinated to two 16-electron metal fragments (ML_n). This fragment analysis and trends in the experimental data parallel bonding analyses of free organopnictane[2] ligands (ER_3) and their metal complexes (ER_3)-ML_n, E = P, As, Sb, and Bi. Accordingly, the term "metallopnictane" is suggested as a descriptor of the $Fe_3(CO)_9(\mu_3\text{-}E)_2$ cluster unit (Figure 1).[3] The key idea that emerges from this study is that the properties of the $Fe_3(CO)_9(\mu_3\text{-}EML_n)_2$ clusters can be rationally tuned by choice of capping ML_n group and heteroatom. In support of these assertions, correlation among structural, spectroscopic, and theoretical results will be presented.

The study of this particular class of clusters is motivated by the discovery of the single two-electron reduction observed for the cluster, $Fe_3(CO)_9[\mu_3\text{-}PMnCp(CO)_2]_2$ (**1-P**), which is associated with the conversion of the *closed* 48-electron triangular cluster to an *open* 50-electron triangular cluster (eq 1).[4] A unique feature of the metallopnictanes is that their net electronic impact (the sum of σ-donating and π-accepting properties) is altered by reduction of the cluster. An understanding of the $Fe_3(CO)_9(\mu_3\text{-}EML_n)_2$ cluster redox properties as a function of heteroatom and capping metal complex will help describe electronic interactions among clusters in chains of $Fe_3(CO)_9$-

⊗ Abstract published in *Advance ACS Abstracts,* October 15, 1997.

(1) (a) Dahl, L. F.; de Gil, E. R.; Feltham, R. D. *J. Am. Chem. Soc.* **1969**, *91*, 1653−1664. (b) Costello, W. R.; King, R. B. *J. Am. Chem. Soc.* **1968**, *90*, 5422−5429. (c) Hoffmann, R.; Fisel, R.; Summerville, R. *J. Am. Chem. Soc.* **1980**, *102*, 4555−4578. (d) Compton, N. A.; Errington, R. J.; Norman, N. C. *Adv. Organomet. Chem.* **1990**, *31*, 91−182. (e) Fehlner, T. P. *Comments Inorg. Chem.* **1988**, *7*, 307−332. (f) Scherer, O. J. *Angew. Chem., Int. Ed. Engl.* **1985**, *24*, 924−943. (g) Scherer, O. *Comments Inorg. Chem.* **1987**, *6*, 1−22. (h) Herrman, W. A. *Angew. Chem., Int. Ed. Engl.* **1986**, *25*, 56−76. (i) Whitmire, K. H. *J. Coord. Chem. B* **1988**, *6*, 95−203.

(2) The IUPAC convention for naming ER_3 groups uses the "ane" suffix instead of the common suffix, "ine." PH_3 is properly called "phosphane" using this convention. Shriver, D. F.; Atkins, P.; Langford, C. H. *Inorganic Chemistry*, 2nd ed.; W. H. Freeman and Co.: New York, 1994.

(3) (a) Bautista, M. T.; White, P. S.; Schauer, C. K. *J. Am. Chem. Soc.* **1991**, *113*, 8963−8965. (b) Huttner refers to $Co_3(CO)_9(\mu_3\text{-}P)$ as a ligand in the cluster $Co_3(CO)_9[\mu_3\text{-}PMnCp(CO)_2]$. Lang, H.; Huttner, G.; Mohr, G.; Sigwarth, B.; Jibril, I.; Zsolnai, L.; Orama, O. *J. Organomet. Chem.* **1986**, *304*, 137−155.

S0020-1669(97)00786-6 CCC: $14.00

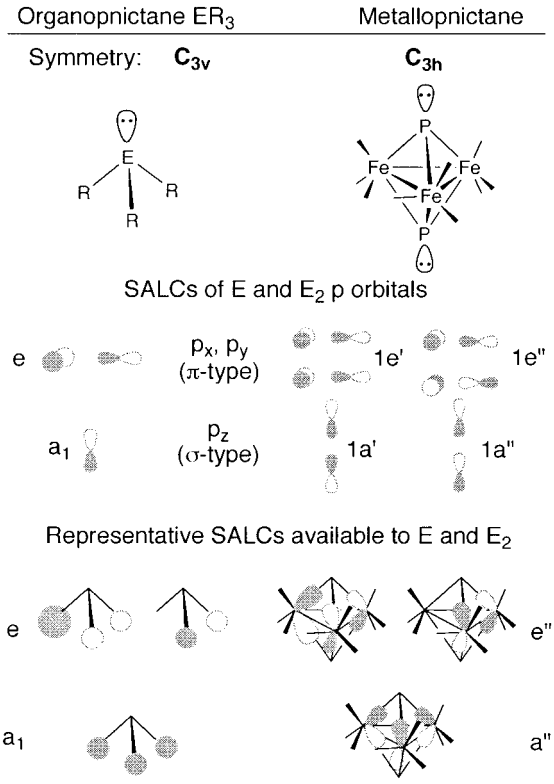

Figure 1. Comparison of an organopnictane and a metallopnictane cluster, including relevant symmetry-adapted linear combinations (SALCs) of orbitals used in bonding.

$(\mu_3\text{-P})_2$ clusters,[4,5] and the design of multielectron redox catalysts based on this system.

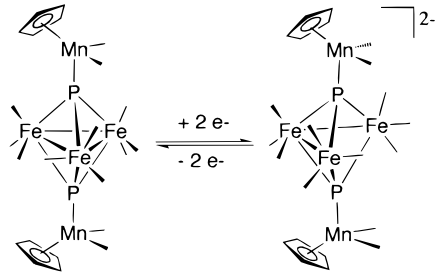

(1)

Results and Discussion

Syntheses and Structures. Huttner and co-workers have reported two general synthetic routes to the bicapped $Fe_3(CO)_9(\mu_3\text{-}EML_n)_2$ clusters.[6] The first route involves reaction of an ECl_3 complex of the capping ML_n group with $Fe_2(CO)_9$, while the second involves reaction of the three-coordinate E(I) complex with the anionic carbonyl, $Na_2Fe(CO)_4$ (Scheme 1).[7] These routes are employed to prepare clusters in the series $Fe_3(CO)_9(\mu_3\text{-}EML_n)_2$ (**1-E**, $ML_n = MnCp(CO)_2$, E = P, As, Sb; **2-E**, $ML_n = Cr(CO)_5$, E = P, As, Sb). Compounds **1-As**, **1-Sb**, and **2-P** have not been previously reported. Both of these routes produce only modest yields of the desired cluster complexes; the first route typically gives larger yields than the second route. The antimony derivatives, **1-Sb** and **2-Sb**, and the As compound,

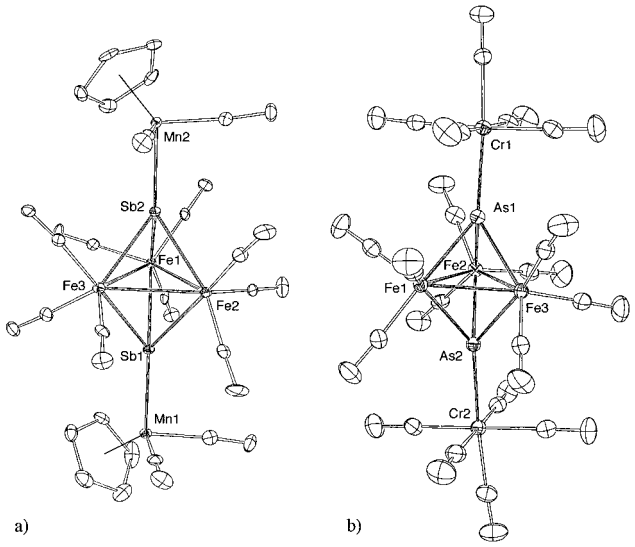

Figure 2. Representative ORTEP diagrams for (a) a series **1** cluster, **1-Sb**, and (b) a series **2** cluster, **2-As**. Thermal ellipsoids are drawn at the 30% probability level.

Scheme 1

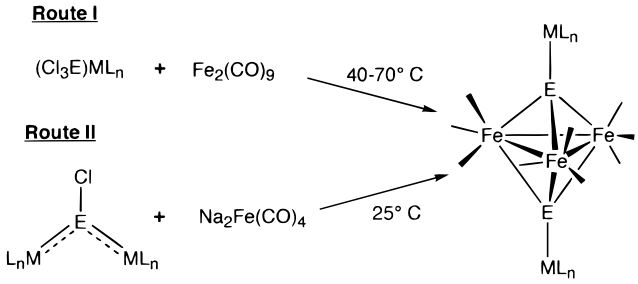

2-As, were only accessible by the second route because the starting ECl_3 complexes of route I are not readily prepared. Syntheses by route II are especially unreliable, and **1-Sb** was only isolated once in several attempts.

Cluster Geometry. The structures of **1-As**, **1-Sb**, **2-P**, **2-As**, and **2-Sb** were characterized by single-crystal X-ray diffraction to determine structural variations as a function of heteroatom and capping metal complex. The structure of **1-P** has been previously reported.[6] All of the clusters examined in this study consist of a triangle of Fe atoms, each with three terminal CO ligands (Figure 2). A group 15 heteroatom caps each face of the triangle. A 16-electron metal fragment, $MnCp(CO)_2$ for series **1** clusters ($Cp = C_5H_5$) and $Cr(CO)_5$ for series **2** clusters, is bound to the heteroatom. In accord with electron-counting rules,[8] three Fe−Fe bonds are observed for the 48-electron trigonal bipyramidal cluster.

The equilibrium geometry observed in the crystal structures is a function of many intra- and intermolecular interactions, and the interpretation of trends in the interatomic distances and angles of these clusters is therefore complex. For example, the $Fe_3(CO)_9(\mu_3\text{-}E)_2$ units in clusters with capping ML_n groups deviate from C_{3h} symmetry reported for analogues without capping ML_n groups bound to the heteroatom ($Fe_3(CO)_9(\mu_3\text{-}E)_2$, E = As[9] and Bi,[10] and $Ru_3(CO)_9(\mu_3\text{-}Bi)_2$[11]). This deviation

(4) Koide, Y.; Bautista, M. T.; White, P. S.; Schauer, C. K. *Inorg. Chem.* **1992**, *31*, 3690−3691.
(5) (a) Bautista, M. T.; White, P. S.; Schauer, C. K. *J. Am. Chem. Soc.* **1994**, *116*, 2143−2144. (b) Jordan, M. R.; White, P. S.; Schauer, C. K.; Mosley, M. A. *J. Am. Chem. Soc.* **1995**, *117*, 5403−5404.
(6) Lang, H.; Huttner, G.; Zsolnai, L.; Mohr, G.; Sigwarth, B.; Weber, U.; Orama, O.; Jibril, I. *J. Organomet. Chem.* **1986**, *304*, 157−179.
(7) The iron reagent $Na_2Fe_2(CO)_8$ can be substituted for $Na_2Fe(CO)_4$. See the Experimental Section.
(8) Mingos, D. M. P. *Acc. Chem. Res.* **1984**, *17*, 311−319. Wade, K. *Adv. Inorg. Chem. Radiochem.* **1976**, *18*, 1−66.
(9) Delbaere, L. T. J.; Kruczynski, L. J.; McBride, D. W. *J. Chem. Soc., Dalton Trans.* **1973**, 307−310.
(10) Churchill, M. R.; Fettinger, J. C.; Whitmire, K. H. *J. Organomet. Chem.* **1985**, *284*, 13−23.
(11) Hay, C. M.; Johnson, B. F. G.; Lewis, J.; Raithby, P. R.; Whitton, A. J. *J. Chem. Soc., Dalton. Trans.* **1988**, 2091−2097.

Table 1. Selected Bond Lengths (Å) and Angles (deg) for $Fe_3(CO)_9(\mu_3\text{-}EML_n)_2$ Clusters (**1** = $MnCp(CO)_2$-Capped; **2** = $Cr(CO)_5$-Capped)[a]

	compound					
	1-P[b]	**1-As**	**1-Sb**	**2-P**	**2-As**	**2-Sb**
Fe1−Fe2	2.604(6)	2.669(2)	2.744(2)	2.582(6)	2.650(2)	2.747(2)
Fe1−Fe3	2.628(6)	2.674(2)	2.763(2)	2.591(6)	2.651(2)	2.758(2)
Fe2−Fe3	2.676(6)	2.737(2)	2.797(2)	2.675(6)	2.762(2)	2.840(2)
Fe−Fe(av)[c]	**2.636(6)**	**2.693(2)**	**2.768(2)**	**2.616(6)**	**2.688(2)**	**2.782(2)**
Fe1−E1	2.281(9)	2.364(2)	2.525(2)	2.281(9)	2.376(2)	2.532(1)
Fe1−E2	2.306(9)	2.387(2)	2.554(2)	2.289(8)	2.396(2)	2.572(2)
Fe2−E1	2.257(9)	2.357(2)	2.526(2)	2.246(9)	2.358(2)	2.532(2)
Fe2−E2	2.259(9)	2.349(2)	2.529(2)	2.202(10)	2.334(2)	2.515(2)
Fe3−E1	2.265(9)	2.367(2)	2.528(2)	2.246(9)	2.353(2)	2.507(1)
Fe3−E2	2.260(9)	2.354(2)	2.525(2)	2.227(8)	2.329(2)	2.501(1)
Fe−E(av)[c]	**2.271(9)**	**2.363(2)**	**2.531(2)**	**2.248(9)**	**2.358(2)**	**2.526(2)**
E1−M1	2.151(9)	2.249(2)	2.426(2)	2.307(9)	2.406(2)	2.552(2)
E2−M2	2.136(9)	2.254(2)	2.417(2)	2.305(9)	2.392(2)	2.550(2)
E−M(av)[c]	**2.144(9)**	**2.251(2)**	**2.421(2)**	**2.306(9)**	**2.399(2)**	**2.551(2)**
E−E	3.37	3.558	3.926	3.326	3.546	3.898
Fe1−Fe2−Fe3	58.8(2)	59.3(1)	59.8(1)	59.0(2)	58.6(1)	59.2(1)
Fe1−Fe3−Fe2	59.7(2)	59.1(1)	59.1(1)	58.7(2)	58.6(1)	58.7(1)
Fe2−Fe1−Fe3	61.5(2)	61.6(1)	61.1(1)	62.3(2)	62.8(1)	62.1(1)
Fe−Fe−Fe(av)[c]	**60.0**	**60.0**	**60.0**	**60.0**	**60.0**	**60.0**
Fe1−E1−Fe2	70.7(3)	68.8(1)	65.8(1)	69.5(3)	68.1(1)	65.7(1)
Fe1−E1−Fe3	70.1(3)	68.8(1)	66.3(1)	69.8(3)	68.2(1)	66.4(1)
Fe2−E1−Fe3	72.6(3)	70.8(1)	67.2(1)	73.1(3)	71.8(1)	68.6(1)
Fe1−E2−Fe2	70.3(3)	68.6(1)	65.3(1)	70.1(3)	68.1(1)	65.3(1)
Fe1−E2−Fe3	69.5(3)	68.6(1)	65.9(1)	70.0(3)	68.2(1)	65.9(1)
Fe2−E2−Fe3	72.6(3)	71.2(1)	67.2(1)	74.3(3)	72.6(1)	69.0(1)
Fe−E−Fe(av)[c]	**71.0(3)**	**69.5(1)**	**66.3(1)**	**71.1(3)**	**69.5(1)**	**66.8(1)**
E1−Fe1−E2	94.5(3)	97.0(1)	101.2(1)	93.4(3)	96.0(1)	99.6(1)
E1−Fe2−E2	96.3(3)	98.2(1)	101.9(1)	96.8(3)	98.2(1)	101.1(1)
E1−Fe3−E2	96.5(3)	97.8(1)	102.0(1)	96.1(3)	98.4(1)	102.2(1)
E−Fe−E(av)[c]	**95.8(3)**	**97.7(1)**	**101.7(1)**	**95.4(3)**	**97.5(1)**	**101.0(1)**

[a] Estimated standard deviations (esd) in the least significant digit(s) are given in parentheses. [b] Data downloaded from the Cambridge Structural Database. The esd values are estimated from ref 6. [c] The numbers reported in parentheses for the average values are calculated by a propagation of random error treatment ($\sqrt{(\sum(\text{esd})^2/n)}$) and represent the estimated standard deviation (esd) in the average value based on the estimated standard deviations in the individual measurements. Shoemaker, D. P.; Garland, C. W.; Steinfeld, J. I.; Nibler, J. W. *Experiments in Physical Chemistry*, 4th ed.; McGraw-Hill Book Co.: New York, 1981; pp 25−55.

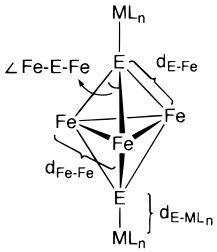

Figure 3. Interatomic distances and angles that are used to describe the bonding in a coordinated metallopnictane.

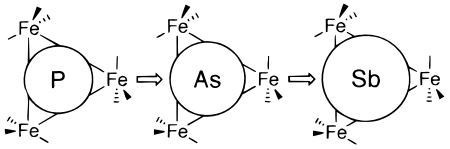

Figure 4. Representation of the mean Fe−Fe distances (drawn to scale) relative to the covalent radius of E. For clarity, the covalent radius for each E is drawn at 80% scale relative to the Fe_3 triangle.

from ideal symmetry is primarily due to steric interactions of the Fe CO ligands and the capping metal ligands.[12] With these precautions noted, the following discussion assumes intramolecular interactions dominate, and the trends in the Fe_3E_2 core measurements are dictated by the Fe−Fe, E−Fe, and E−E interactions (Figure 3). Average interatomic distances and angles are used for comparison among these clusters even though there is significant variance in some of the data.

(a) Geometry and Heteroatom Size: E−Fe and Fe−Fe Bonding. All internal Fe_3E_2 core distances increase with increasing heteroatom covalent radius (Table 1, Figure 4).[13] The observed heteroatom−iron (E−Fe) distances are very close to the values predicted from single-bond covalent radii (P−Fe 2.265 Å; As−Fe 2.375 Å; Sb−Fe 2.575 Å).[14] A less pronounced increase in the mean Fe−Fe distance is observed with the covalent radius of the capping heteroatom. Similar Fe−Fe distances are observed for clusters that have the same heteroatom but different capping ML_n groups (Fe−Fe(av) = 2.63 Å, E = P; 2.69 Å, E = As; 2.77 Å, E = Sb). The E−E distances are near to the sum of their van der Waals radii; accordingly, the E−E interactions are not considered to be a dominant factor in determining the Fe_3E_2 geometry.[15] These trends between internal M_3E_2 interatomic distances and angles and covalent radius of E hold for other series of heteroatom capped clusters (Table 2).[16] The linear correlation between heteroatom covalent

(12) Haupt and Flörke attribute minimization of intra- and intermolecular repulsive forces in the packing of $Fe_3(CO)_9[\mu_3\text{-}GeRe(CO)_5]_2$ to the equilibrium of C−O, C−C, and O−O contacts as an explanation for the differing Fe−Fe−Fe and Fe−Ge−Fe bond angles and metal−metal bond lengths in this cluster. Haupt, H.-J. and Flörke, U. *Acta Crystallogr.* **1988**, *C44*, 472−474.

(13) Anema, S. G.; Mackay, K. M.; Nicholson, B. K.; Van Tiel, M. *Organometallics* **1990**, *9*, 2436−2442.

(14) Pauling, L. *The Nature of the Chemical Bond*, 3rd ed.; Cornell University Press: Ithaca, NY, 1960; Chapter 7.

(15) Kahlal, S.; Halet, J.-F.; Saillard, J.-Y.; Whitmire, K. H. *J. Organomet. Chem.* **1994**, *478*, 1−8.

Table 2. Average Interatomic Distances and Angles for $Fe_3(CO)_9(\mu_3\text{-}EML_n)_2$ and Related 48-Electron Clusters[a]

cluster	Fe−Fe (Å)	Fe−E (Å)	E−ML_n (Å)	Fe−E−Fe (deg)
$Fe_3(CO)_9(\mu_3\text{-}CF)_2$[b,c]	2.540(2)	1.922(8)	1.354(4)	83.3(2)
$Fe_3(CO)_8(PMe_3)(\mu_3\text{-}CF)_2$[d]	2.530(2)	1.91(1)	1.35(1)	82.8(6)
$Fe_3(CO)_9[\mu_3\text{-}PMnCp(CO)_2]_2$ (**1-P**)[e]	2.636(6)	2.271(9)	2.144(9)	71.0(3)
$Fe_3(CO)_9[\mu_3\text{-}PMnCp(CO)_2][\mu_3\text{-}PFe(CO)_4]$ (**3-P**)[e,f]	2.660(5)	2.281(8)	2.191(8)	71.4(2)
		2.244(8)	2.217(8)	72.7(2)
$Fe_3(CO)_9[\mu_3\text{-}PCr(CO)_5][\mu_3\text{-}PFe(CO)_4]$[e,f]	2.630(3)[c]	2.225(2)[c]	2.301(4)	72.5(1)[c]
			2.163(4)	
$Fe_3(CO)_9[\mu_3\text{-}PCr(CO)_5]_2$ (**2-P**)	2.616(6)	2.248(9)	2.306(9)	71.1(3)
$Fe_3(CO)_6[P(OR)_3]_3[\mu_3\text{-}PMnCp(CO)_2](\mu_3\text{-}P)$[e,f]	2.617(2)	2.238(2)	2.166(3)	72.1(1)
		2.235(3)		71.7(1)
$Fe_3(CO)_9[\mu_3\text{-}SiFeCp(CO)_2]_2$[g]	2.667(1)	2.306(1)	2.251(1)	70.6(1)
$Fe_3(CO)_9(\mu_3\text{-}As)_2$[h]	2.623(7)	2.348(3)		67.9(1)
$Fe_3(CO)_9[\mu_3\text{-}AsMnCp(CO)_2]_2$ (**1-As**)	2.693(2)	2.363(2)	2.251(2)	69.5(1)
$Fe_3(CO)_9[\mu_3\text{-}AsCr(CO)_5]_2$ (**2-As**)	2.688(2)	2.358(2)	2.399(2)	69.5(1)
$Fe_3(CO)_9(\mu_3\text{-}GeCH_2CH_3)_2$[g]	2.738(3)	2.326(3)	1.940(4)	72.1(1)
$Fe_3(CO)_9[\mu_3\text{-}GeFeCp(CO)_2]_2$[g]	2.726(2)	2.378(2)	2.318(2)	70.0(1)
$Fe_3(CO)_9[\mu_3\text{-}GeRe(CO)_5]_2$[i]	2.718(4)	2.379(4)	2.542(3)	69.7(1)
$Fe_3(CO)_9[\mu_3\text{-}SbMnCp(CO)_2]_2$ (**1-Sb**)	2.768(2)	2.531(2)	2.421(2)	66.3(1)
$Fe_3(CO)_9[\mu_3\text{-}SbCr(CO)_5]_2$ (**2-Sb**)	2.782(2)	2.526(2)	2.551(2)	66.8(1)
$Fe_3(CO)_9[\mu_3\text{-}SnFeCp(CO)_2]_2$[j]	2.792(3)	2.537(2)	2.471(4)	66.8(1)
$Fe_3(CO)_9[\mu_3\text{-}SnRe(CO)_5]_2$[k]	2.807(2)	2.543(3)	2.726(2)	67.0(1)
$Fe_3(CO)_9[\mu_3\text{-}SnMn(CO)_5]_2$[l,m]	2.81	2.54	2.60	67.2
$Fe_3(CO)_9(\mu_3\text{-}Bi)_2$[n]	2.745(5)	2.628(2)		63.0(1)
$Ru_3(CO)_9(\mu_3\text{-}Bi)_2$[o]	2.930(2)	2.750(2)		64.4(1)

[a] Metric parameters were downloaded from the Cambridge Structural Database. The number reported in parentheses is $\sqrt{(\sum(\text{esd})^2/n)}$ (Table 1, footnote *c*). [b] Lentz, D.; Brüdgam, I.; Hartl, H. *Angew. Chem., Int. Ed. Engl.* **1985**, *24*, 119−120. [c] Average metric parameters and esd's are estimated from data ranges reported in the reference. [d] Lentz, D.; Michael-Schulz, H. *Z. Anorg. Allg. Chem.* **1992**, *618*, 111−120. [e] Reference 6. [f] Average metric parameters for each side of the triiron triangle are listed in the order they are given in the compound. [g] Anema, S. G.; Mackay, K. M.; Nicholson, B. K.; Van Tiel, M. *Organometallics* **1990**, *9*, 2436−2442. [h] Reference 9. [i] Reference 12. [j] McNeese, T. J.; Wreford, S. S.; Tipton, D. L.; Bau, R. *J. Chem. Soc., Chem. Commun.* **1977**, 390−391. [k] Haupt, H.-J.; Gotze, A.; Flörke, U. Z. *Z. Anorg. Allg. Chem.* **1988**, *557*, 82−90. [l] Flörke, U.; Haupt, H.-J. *Z. Kristallogr.* **1992**, *201*, 301−303. [m] Estimated standard deviations are not reported. [n] Reference 10. [o] Reference 11.

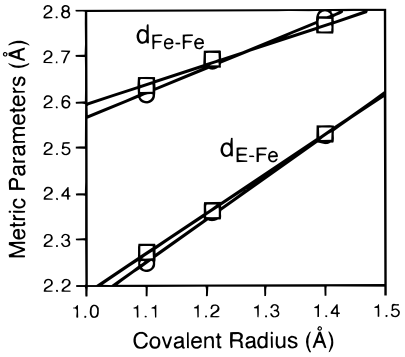

Figure 5. Correlation of Fe−Fe and E−Fe distances with heteroatom covalent radius for series **1** (□) and series **2** (○) clusters.

radius and the E−Fe and Fe−Fe distances for series **1** and series **2** clusters are presented in Figure 5.

The Fe−E−Fe bond angle in the $Fe_3(CO)_9(\mu_3\text{-}EML_n)_2$ clusters decreases as a larger heteroatom is incorporated into the Fe_3E_2 framework (average of series **1** and **2**: Sb (67°) < As (70°) < P (71°)). An analogous trend is observed in free organo-ER_3 (organopnictane) ligands as a function of heteroatom, in which the average $C_{ipso}-E-C_{ipso}$ bond angle decreases from 103.0° in PPh_3 to 100.2° in $AsPh_3$ to 96.0° in $SbPh_3$ (Table 3). The cluster angles are smaller than the organopnictane angles because of bonding interactions between the Fe atoms, and presumably the Fe−Fe bonding moderates the intrinsic bonding preferences of the heteroatom. Smaller M−E−M angles in dinuclear complexes have been used to infer stronger metal−metal interactions in dinuclear species with different types of bridging ligands.[1c] The fact that the variation in the M−E−M bond angle in the metallopnictane system as a function of heteroatom mirrors those for EPh_3 groups suggests that interpretations of changes in the strength of the Fe−Fe interactions as the heteroatom is changed based on this measure are not straightforward in this system.

Structural data are available for the uncoordinated metalloarsane ligand, $Fe_3(CO)_9(\mu_3\text{-}As)_2$. The Fe−As−Fe bond angle of the metalloarsane $Fe_3(CO)_9(\mu_3\text{-}As)_2$ increases by about 1.5° upon coordination to the ML_n capping groups $MnCp(CO)_2$ (**1-As**) and $Cr(CO)_5$ (**2-As**). A similar magnitude increase in C−E−C angle is observed for the larger heteroatoms upon EPh_3 coordination

Table 3. Average Interatomic Distances and Angles for EPh_3 and $(EPh_3)Cr(CO)_5$[a]

E	Cr−E (Å)	C−E−C (deg)	E−C (Å)
PPh_3[b]		102.8(1)	1.831(2)
$(PPh_3)Cr(CO)_5$[c]	2.422(1)	102.6(2)	1.828(3)
$AsPh_3$[d]		100.1(3)	1.957(7)
$(AsPh_3)Cr(CO)_5$[e]	2.497(1)	101.4(1)	1.947(3)
$SbPh_3$[f]		96.3(3)	2.155(7)
$(SbPh_3)Cr(CO)_5$[e]	2.617(0)	99.8(1)	2.133(2)
$BiPh_3$[g]		93.9(2)	2.259(8)
$(BiPh_3)Cr(CO)_5$[e]	2.705(1)	98.7(3)	2.216(9)

[a] The number reported in parentheses is $\sqrt{(\sum(\text{esd})^2/n)}$ (Table 1, footnote *c*). [b] Dunne, B. J.; Orpen, A. G. *Acta Crystallogr.* **1991**, *C47*, 345−347. [c] Plastas, H. J.; Stewart, J. M.; Grim, S. O. *Inorg. Chem.* **1972**, *12*, 265−272. [d] Sobolev, A. N.; Belsky, V. K.; Chernikova, N. Yu.; Akhmadulina, F. Yu. *J. Organomet. Chem.* **1983**, *244*, 129−136. [e] Carty, A. J.; Taylor, N. J.; Coleman, A. C.; Lappert, M. F. *J. Chem. Soc., Chem. Commun.* **1979**, 639−640. [f] Adams, E. A.; Kolis, J. W.; Pennington, W. T. *Acta Crystallogr.* **1990**, *C46*, 917−919. [g] Jones, P. G.; Blaschete, A.; Henschel, D.; Weitze, A. *Z. Kristallogr.* **1995**, *210*, 377−378.

(16) Similar trends in M−E−M angle have been characterized for open 50-electron clusters $Fe_3(CO)_9(\mu_3\text{-}ER)_2$. Eveland, J. R.; Saillard, J.-Y.; Whitmire, K. H. *Inorg. Chem.* **1997**, *36*, 330−334.

Table 4. Comparison of the Metallopnictane E−ML_n Distances with Organopnictane Compounds

pnictane	ML_n	E−M[a] (Å)
PCl_3[b]	$Cr(CO)_5$	2.24
PBr_3[b,c]	$Cr(CO)_5$	2.25/2.26
$P[Fe(CO)_3]_3P$ (**2-P**)	$Cr(CO)_5$	2.31
PH_3[d]	$Cr(CO)_5$	2.35
PPh_3[e]	$Cr(CO)_5$	2.42
$As[Fe(CO)_3]_3As$ (**2-As**)	$Cr(CO)_5$	2.40
$AsPh_3$[f]	$Cr(CO)_5$	2.50
$Sb[Fe(CO)_3]_3Sb$ (**2-Sb**)	$Cr(CO)_5$	2.55
$SbMeBr_2$[g]	$Cr(CO)_5$	2.56
$SbPh_3$[f]	$Cr(CO)_5$	2.62
$P[Fe(CO)_3]_3P$ (**1-P**)	$MnCp(CO)_2$	2.14
$P(SPh)_3$[h]	$MnCp(CO)_2$	2.17
PPh_3[i]	$MnCp(CO)_2$	2.24
$[P[Fe(CO)_3]_3P]^{2-}$ $(\mathbf{1\text{-}P})^{2-}$	$MnCp(CO)_2$	2.25

[a] The estimated standard deviations for each of these measures is typically less than 0.002 Å and are omitted. [b] Davies, M. S.; Aroney, M. J.; Buys, I. E.; Hambley, T. W.; Calvert, J. L. *Inorg. Chem.* **1995**, *34*, 330−336. [c] Jelinek-Fink, H.; Duesler, E. N.; Paine, R. T. *Acta Crystallogr.* **1987**, *C43*, 635−636. [d] Huttner, G.; Shelle, S. *J. Organomet. Chem.* **1973**, *47*, 383−390. [e] Plastas, H. J.; Stewart, J. M.; Grim, S. O. *Inorg. Chem.* **1973**, *12*, 265−272. [f] Carty, A. J.; Taylor, N. J.; Coleman, A. W.; Lappert, M. F. *J. Chem. Soc. Chem. Commun.* **1973**, 639−640. [g] Breunig, H. J.; Denker, M.; Ebert, K. H. *J. Organomet. Chem.* **1994**, *470*, 87−92. [h] Sinyashin, O. G.; Gorshunov, I. Yu.; Milukov, V. A.; Batyeva, E. S.; Litvinov, I. A.; Kataeva, O. N.; Ginzburg, A. G.; Sokolov, V. I. *Russ. Chem. Bull.* **1994**, *43*, 1054−1057. [i] Barbeau, C.; Dichmann, K. S.; Ricard, L. *Can. J. Chem.* **1973**, *51*, 3027−3031.

to a metal complex (Table 3). The As−Fe distance and Fe−Fe distance increase slightly upon coordination of $Fe_3(CO)_9(\mu_3\text{-}As)_2$, but the influence of steric interactions between the capping metal complex and the cluster core hamper interpretation of these small changes in distances.

(b) E−ML_n Bonding. The distances between the triply-bridging heteroatom E and the appended ML_n group also display the expected linear correlation with the size of E (Table 1). Comparisons of the E−ML_n distances for the metallopnictanes to organo- and halopnictane analogues, $L_nM(ER_3)$, and bonding descriptions of $L_nM(ER_3)$ complexes[17] allow assessment of the nature of the interaction between the metallopnictane ligand and a capping metal complex. The E−Cr distances in series **2** are ∼0.1 Å shorter than in the analogous $Cr(CO)_5(EPh_3)$ complexes (Table 4). Likewise, the P−Mn distance in **1-P** (Table 4) is 0.08 Å shorter than for $MnCp(CO)_2(PPh_3)$ (Mn−P = 2.236 (3) Å). The E−ML_n bond lengths observed in the $Fe_3(CO)_9(\mu_3\text{-}EML_n)_2$ clusters suggest that both lone pair donation of E to the capping ML_n group and L_nM-to-$E_2Fe_3(CO)_9$ π-back-bonding interactions are important in E−M bonding. The E−M distances are not as short as trihalopnictane $ML_n(EX_3)$ analogues (Table 4), implying that the metallopnictanes are intermediate between organopnictanes and halopnictanes in terms of their net electronic impact (the sum of σ-donating and π-accepting properties).

Infrared Spectroscopy. The CO ligands on the triiron core and the capping ML_n group provide a powerful tool to probe the changes in electron density in the $Fe_3(CO)_9(\mu_3\text{-}EML_n)_2$ clusters as a function of E and ML_n. In general, an increase in the net electron density at a metal site results in lower CO stretching frequencies for the appended CO ligands.[18] A comparison of the patterns observed in the CO stretching region of the infrared spectrum among the series **1** and series **2** clusters (Figure 6) has enabled modes to be assigned to the Fe_3 core or the ML_n cap (Table 5). For the series **2** clusters, three bands (2064, ∼1982, 1969 cm^{-1}) stay relatively constant in energy while two change upon heteroatom substitution (Figure 7). The three invariant bands are assigned to the capping $Cr(CO)_5$ fragment on the basis of the CO stretching data for the complexes $M(CO)_5(EPh_3)$ (M = Cr[19] and Mo;[20] E = P, As, and Sb). The remaining two bands are assigned to the Fe_3-core CO stretches. To confirm these assignments, a sample of **2-P** enriched with ^{13}CO at the Fe_3 core was prepared by stirring **2-P** under an atmosphere of ^{13}CO in the presence of a catalytic amount of a reducing agent.[21] In the spectrum of partially enriched **2-P**, the bands assigned to the $Cr(CO)_5$ cap remain sharp, while those assigned to the Fe_3 core broaden upon ^{13}CO substitution. A similar analysis of the series **1** spectra shows that the frequencies of the two lowest energy stretching modes stay relatively constant as the capping heteroatom is changed (Figure 7), and accordingly, they are assigned to the capping $MnCp(CO)_2$ groups.

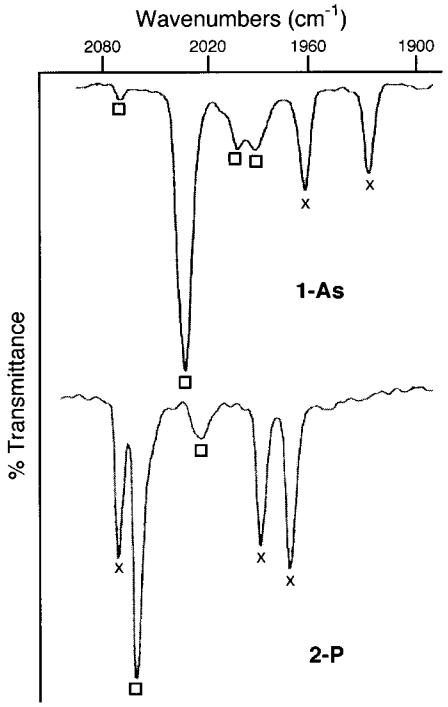

Figure 6. Representative IR spectra in the CO stretching region for $MnCp(CO)_2$-capped (**1-As**) and for $Cr(CO)_5$-capped (**2-P**) clusters. The CO stretching modes assigned to the $Fe_3(CO)_9$ core (□) and the ML_n cap stretches (×) are indicated.

An examination of Figure 7 shows a different pattern of Fe_3-core CO stretching modes is observed for series **1** and series **2** clusters; four bands are observed for series **1** clusters while two bands are observed for series **2** clusters. The pattern of Fe_3-core CO stretching modes for the series **2** clusters closely resembles the pattern for the naked cluster $Fe_3(CO)_9(\mu_3\text{-}E)_2$, E = As and Bi. One possible explanation for the different patterns is the electronic asymmetry of the a′ and a″ Mn dπ orbitals of the C_s symmetric $MnCp(CO)_2$ capping group.[22]

(17) (a) Xiao, S.-X.; Trogler, W. C.; Ellis, D. E.; Berkovitch-Yellin, Z. *J. Am. Chem. Soc.* **1983**, *105*, 7033−7037. (b) Davies, M. S.; Aroney, M. J.; Buys, I. E.; Hambley, T. W.; Calvert, J. L. *Inorg. Chem.* **1995**, *34*, 330−336. (c) Pacchioni, G.; Bagus, P. S. *Inorg. Chem.* **1992**, *31*, 4391−4398. (d) Gilheany, D. G. *Chem. Rev.* **1994**, *94*, 1339−1374.

(18) (a) Cotton, F. A. and Wilkinson, G. *Advanced Inorganic Chemistry*, 5th ed.; John Wiley & Sons: New York, 1994; pp 58−64. (b) Goldman, A. S.; Krough-Jespersen, K. *J. Am. Chem. Soc.* **1996**, *118*, 12159−12166 and references therein.

(19) Cotton, F. A.; Kraihanzel, C. S. *J. Am. Chem. Soc.* **1962**, *84*, 4432−4438.

(20) Darensbourg, D. J.; Brown, T. L. *Inorg. Chem.* **1968**, *7*, 959−966.

(21) Koide, Y.; Schauer, C. K. *Organometallics* **1993**, *12*, 4854−4862.

Table 5. Infrared CO Stretching Frequencies[a]

cluster $Fe_3(CO)_9(EML_n)_2$ EML_n =	Fe core carbonyl str freq (cm^{-1})	capping metal carbonyl str freq (cm^{-1})
$PMnCp(CO)_2$ (**1-P**)	2074 (vw), 2036 (s), 2008(w), 1996(w,sh)	1968 (m), 1929 (m)
$AsMnCp(CO)_2$ (**1-As**)	2068 (vw), 2031 (s), 2002 (w), 1990 (w)	1965 (m), 1928 (m)
$SbMnCp(CO)_2$ (**1-Sb**)	2058 (vw), 2023 (s), 1990 (w), 1979 (w)	1963 (m), 1926 (m)
$PCr(CO)_5$ (**2-P**)	2054 (s), 2019 (w)	2064 (m), 1985 (m), 1968 (m)
$AsCr(CO)_5$ (**2-As**)	2048 (s), 2011 (w)	2064 (m), 1980 (m), 1969 (m)
$SbCr(CO)_5$ (**2-Sb**)	2037 (s), 1996 (w)	2064 (m), 1982 (m), 1969 (m)
As[b]	2035 (vs), 2005 (w)	
Bi[c]	2012 (vs), 1969 (w)	

[a] All data are collected on pentane solutions. Abbreviations: vs = very strong, s = strong, m = medium, w = weak, vw = very weak, sh = shoulder. [b] Zimler, T.; Vizi-Orosz, A.; Markó, L. *Transition Met. Chem.* **1977**, *2*, 97−99. [c] Reference 10.

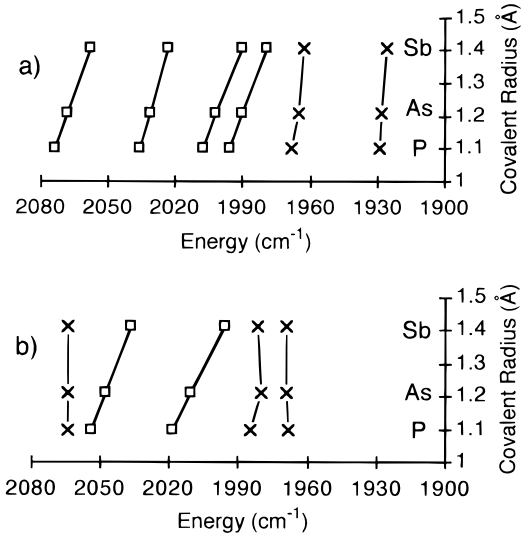

Figure 7. Infrared CO stretching frequencies as a function of E for (a) series **1** and (b) series **2** clusters. The CO stretching modes assigned to the $Fe_3(CO)_9$ core (□) and ML_n cap (×) are indicated.

The electronic properties of both the heteroatom, E, and capping ML_n group influence the Fe_3-core electron density as measured by the Fe_3-core CO stretching frequencies. The Fe_3-core CO stretching frequencies decrease in energy ∼15 cm^{-1} through the series P to As to Sb, similar to the trend observed for the uncoordinated clusters $Fe_3(CO)_9(\mu_3\text{-}E)_2$ (E = As,[9] Bi[10]). These data are consistent with the relative electronegativities of the heteroatoms. Phosphorus is the most electronegative capping heteroatom,[23] and therefore more electron density is delocalized from the $Fe(CO)_3$ groups to the capping heteroatom when E = P.

The influence of the different ML_n caps on the electron density at the $Fe_3(CO)_9$ core is less straightforward to extract given the different pattern of CO stretching modes. The strongest Fe_3-core CO stretching modes in the series **1** clusters are consistently to lower frequency than the analogous cluster in series **2**. For example, the strongest Fe_3-core CO stretching mode for **1-P** (2036 cm^{-1}) lies 18 cm^{-1} to lower energy than the corresponding mode in **2-P** (2054 cm^{-1}). Interestingly, the strongest Fe_3-core CO stretch for the uncoordinated cluster $Fe_3(CO)_9(\mu_3\text{-}As)_2$ (2035 cm^{-1}) lies in between the stretches for the $Cr(CO)_5$-capped cluster (2048 cm^{-1}) and the cluster capped with $MnCp(CO)_2$ (2031 cm^{-1}). This trend suggests that the $Cr(CO)_5$ group is the *net* electron-withdrawing in comparison to the $MnCp(CO)_2$ group.[24]

Table 6. Comparison of Metallophosphane and ER_3 Ligand Influence on $MnCp(CO)_2L$ and $Cr(CO)_5L$ CO Stretching Frequencies[a]

L =	$MnCp(CO)_2L$ ν_{CO} (cm^{-1})
CO	2029 (s), 1947 (s)
PCl_3	1996 (s), 1947 (s)
$PFe_3(CO)_9PFe(CO)_4$ (**3-P**)	1963 (m), 1936 (m)
$PFe_3(CO)_9PMnCp(CO)_2$ (**1-P**)	1964 (m), 1926 (m)
PPh_3	1947 (s), 1884 (s)

L =	$Cr(CO)_5L$ ν_{CO} (cm^{-1})
PCl_3	2089 (m), 2002 (s), 1984 (vs), [1954 (vw)]
$PFe_3(CO)_9PCr(CO)_5$ (**2-P**)	2064 (m), 1985 (m), 1968 (m)
PPh_3[b]	2064 (w), 1987 (s), 1945 (w)

[a] All data are collected on pentane solutions. Data was compared to literature values when appropriate. Abbreviations: vs = very strong, s = strong, m = medium, w = weak, vw = very weak, sh = shoulder. [b] Reference 19.

It was shown above that the E−ML_n bond distances for the metallopnictanes lie in between those for halophosphanes and alkyl- or arylphosphanes. The electronic impact of the metallopnictanes relative to organo-ER_3 ligands based on the E−ML_n distances is supported by the CO stretching frequencies of the capping ML_n groups (Table 6). For $MnCp(CO)_2L$ complexes, the CO stretching frequencies are at the highest energy for L = PCl_3 (1987 cm^{-1}, 1933 cm^{-1}), intermediate for **1-P**, L = $P[Fe_3(CO)_9[\mu_3\text{-}PMnCp(CO)_2]$ (1959 cm^{-1}, 1915 cm^{-1}), and at the lowest energy for L = PPh_3 (1947, 1884 cm^{-1}). In the unsymmetrical capped cluster $Fe_3(CO)_9[\mu_3\text{-}PMnCp(CO)_2][\mu_3\text{-}PFe(CO)_4]$ (**3-P**),[6] the electron-withdrawing nature of the $Fe(CO)_4$ fragment is communicated through the $Fe_3(CO)_9(\mu_3\text{-}P)_2$ cluster unit to the $MnCp(CO)_2$ group bound to the opposite heteroatom. The average of the Mn CO stretching frequencies for **3-P** lies 5 cm^{-1} to higher energy than the average for **1-P**. Analogous trends are observed for $Cr(CO)_5L$ complexes (Table 6).

Cyclic Voltammetry. This study was initiated to better understand the electrochemistry of the cluster $Fe_3(CO)_9[\mu_3\text{-}PMnCp(CO)_2]_2$ (**1-P**), which undergoes a reversible two-electron reduction observed as a single wave in the cyclic voltammogram.[4] The two-electron reduction is coupled with a structural change in which one Fe−Fe bond in neutral **1-P** is cleaved as shown in the crystal structure of $[(PhCH_2)Me_3N]_2$(**1-P**) (Figure 8; Table 7). This result is consistent with electron-counting rules; 48-electron clusters have closed (*closo*) geometries whereas 50-electron clusters have an open (*nido*) geometry.[8] Calculations and previous results[4] suggest the localized Fe−Fe bond cleavage observed in $(\mathbf{1\text{-}P})^{2-}$ results from a second-order Jahn−Teller distortion upon occupation of orbitals in **1-P** that are strongly Fe−Fe antibonding.

(22) For a bonding description of $MnCp(CO)_2L$, see: Schilling, B. E. R.; Hoffmann, R.; Lichtenberger, D. L. *J. Am. Chem. Soc.* **1979**, *101*, 585−591.
(23) Reference 2, pp 43−46.
(24) Lichtenberger, D. L.; Fenske, R. F. *Inorg. Chem.* **1976**, *15*, 2015−2022.

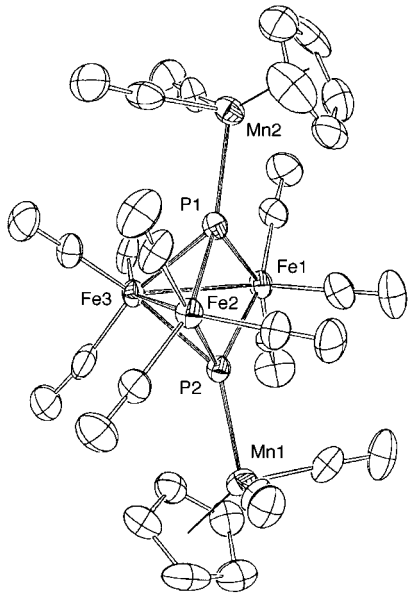

Figure 8. ORTEP diagram of $(\mathbf{1\text{-}P})^{2-}$. Thermal ellipsoids are drawn at the 30% probability level.

Table 7. Selected Interatomic Distances and Angles for $[(PhCH_2)Me_3N)]_2\{Fe_3(CO)_9[\mu_3\text{-}PMnCp(CO)_2]_2\}$ $[(\mathbf{1\text{-}P})^{2-}]^a$

bond lengths (Å)		bond angles (deg)	
Fe1−Fe3	2.653(2)	Fe1−Fe3−Fe2	83.05(7)
Fe2−Fe3	2.634(3)	Fe2−Fe1−Fe3	48.24(6)
Fe1···Fe2	3.596(2)	Fe1−Fe2−Fe3	48.70(6)
Fe−Fe(av)[b]	**2.961(2)**	**Fe−Fe−Fe(av)**	**60.0**
Fe1−P1	2.256(3)	Fe1−P1−Fe2	101.8(1)
Fe2−P1	2.261(4)	Fe1−P1−Fe3	72.0(1)
Fe3−P1	2.261(4)	Fe2−P1−Fe3	71.3(1)
Fe1−P2	2.248(3)	Fe1−P2−Fe2	101.8(2)
Fe2−P2	2.269(4)	Fe1−P2−Fe3	71.9(1)
Fe3−P2	2.273(3)	Fe2−P2−Fe3	70.9(1)
Fe−P(av)	**2.261(4)**	**Fe−P−Fe(av)**	**81.6(1)**
P1−Mn2	2.270(4)	P1−Fe1−P2	77.5(1)
P2−Mn1	2.233(4)	P1−Fe2−P2	77.0(1)
P−Mn(av)	**2.252(4)**	P1−Fe3−P2	76.9(1)
P···P	**2.819(4)**	**E−Fe−E(av)**	**77.1(1)**

[a] Estimated standard deviations (esd) in the least significant digit(s) are given in parentheses. [b] The number reported in parentheses ($=\Sigma\sqrt{(esd)^2}$) is an estimate of the error associated with the average value: See reference in Table 1, footnote *c*.

Table 8. Electrochemical Parameters for Two-Electron Reduction Waves

$E_{1/2}$ vs Fc^+/Fc Couple (mV)	P	As	Sb
series **1**[a]	−895	−800	−690
series **1**[b]	−1050	−995	
series **2**[b]	−660	−600	−510

[a] Cyclic voltammograms were recorded in CH_3CN. [b] Cyclic voltammograms were recorded in CH_2Cl_2. The potentials were referenced to an internal standard, the $Fc^{+/0}$ redox couple.

All of the $Fe_3(CO)_9(\mu_3\text{-}EML_n)_2$ clusters in this study show a two-electron reduction that appears as a single-wave in the cyclic voltammogram (Table 8). The two-electron reductive behavior was established by corrected peak separations and wave shapes. For **2-As** and **1-Sb**, infrared spectroelectrochemistry experiments were conducted.[25] The patterns of CO stretching modes for the doubly reduced species are consistent with an open geometry (two Fe−Fe bonds; pseudo C_{2v} symmetry) and a dinegative charge; the CO stretching frequencies of $(\mathbf{1\text{-}P})^{2-}$ are ∼60 cm^{-1} to lower energy than the neutral parent.

(25) See Supporting Information.

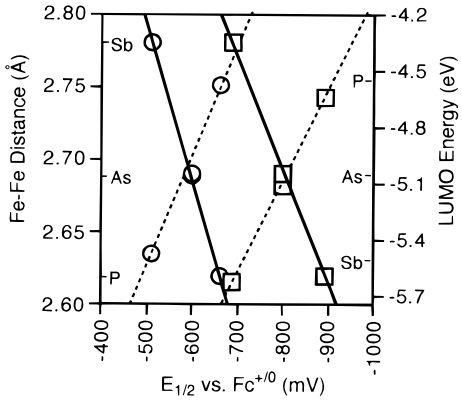

Figure 9. Correlation between (1) redox potential ($E_{1/2}$) and Fe−Fe distance (solid lines) and (2) redox potential and LUMO energy (dashed lines) for series **1** (□) and **2** (○) clusters.

For both series **1** and **2** clusters, the $E_{1/2}$ values linearly correlate with the capping heteroatom covalent radius (and the corresponding Fe−Fe distance), with the $E_{1/2}$ value for the antimony-capped clusters lying at the most positive potentials. The potential range spanned by the three members of each series is ∼150 mV (Table 8). The LUMOs of the 48-electron clusters are strongly Fe−Fe antibonding, and as expected, the LUMO energies decrease as the Fe−Fe distance increases to accommodate a larger E heteroatom (Figure 9). The trend in $E_{1/2}$ values as a function of E is opposite from what would be predicted on the basis of the trend in Fe_3 core CO stretching frequencies. Sb-capped clusters have the most electron density on the Fe_3-core but are reduced at the most positive potentials. The primary factor in establishing the $E_{1/2}$ data trend is the correlation between LUMO energy and heteroatom size (Fe−Fe distance).

The electronic nature of the capping metal fragment has a major influence on the $E_{1/2}$ values. The series **2** clusters are reduced at potentials ∼400 mV more positive than the analogous series **1** clusters, reflecting the relative electron-withdrawing nature of the $Cr(CO)_5$ cap versus the $MnCp(CO)_2$ cap (Table 8). These data are compatible with the infrared spectroscopy measurements of the electron density at the Fe_3 core as a function of ML_n.

Fenske−Hall Molecular Orbital Calculations. Fenske−Hall calculations[26] were performed on both the $Fe_3(CO)_9(\mu_3\text{-}EML_n)_2$ clusters and the corresponding uncapped $Fe_3(CO)_9(\mu_3\text{-}E)_2$ clusters to attain a qualitative understanding of the bonding features in this system. These calculations will be presented in detail elsewhere, but an analysis of the changes in bonding resulting from a change in heteroatom together with analogies to organopnictane (ER_3) ligands is presented here. Idealized C_{3h} symmetry structures are used in the calculations, and the interatomic distances and angles are set to a representative value for a given heteroatom on the basis of the experimental structural data.

(a) Uncapped Cluster Bonding. The molecular orbital (MO) diagram for $Fe_3(CO)_9(\mu_3\text{-}P)_2$ in C_{3h} symmetry highlights the interaction of the two capping heteroatoms with the metal cluster face (Figure 10).[27] The $Fe_3(CO)_9$ fragment orbitals fall into two sets: the t_{2g}-like set (1a′ → 2e′) and the e_g-like set (3e′ → 4e′). The names for the orbital sets are derived from the octahedral-like splitting of Fe 3d orbitals in the $Fe(CO)_3$ fragment.[28] The e_g-like set also includes the 3a′ and 4e′ orbitals that contain a large degree of Fe 4s and 4p character. For the

(26) Hall, M. B.; Fenske, R. F. *Inorg. Chem.* **1972**, *11*, 768−775. Fenske, R. F. *Pure Appl. Chem.* **1971**, *27*, 61−71.

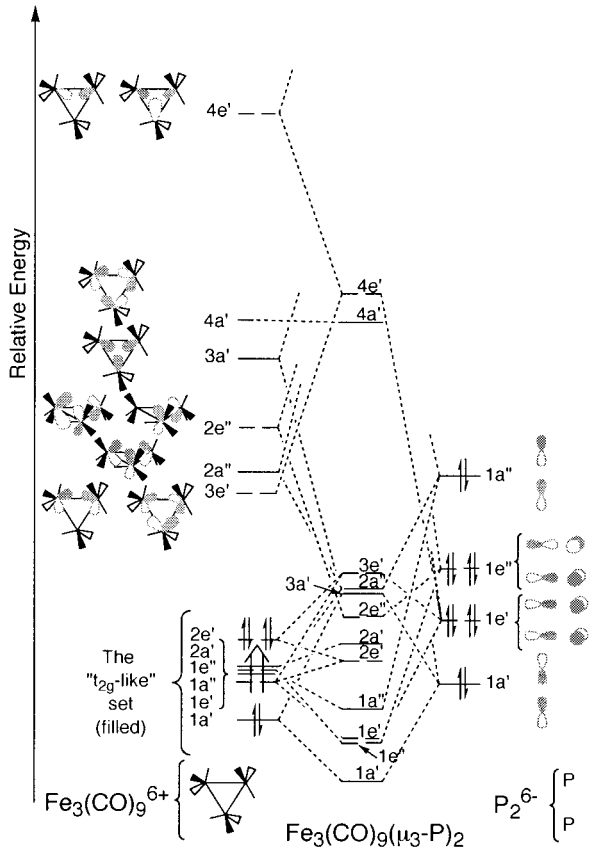

Figure 10. MO diagram for $Fe_3(CO)_9(\mu_3\text{-}P)_2$ illustrating the important P_2-Fe_3 interactions. The Fe_3 triangle for the $Fe_3(CO)_9$ fragment is drawn in the plane of the paper for the (′) orbitals and perpendicular to the page for the (″) e_g-like orbital set. The P···P axis is in the plane of the paper. Symmetry labels are from the C_{3h} point group.

sake of discussion, the bonding in the $Fe_3(CO)_9(\mu_3\text{-}P)_2$ cluster is described in terms of interaction of a P_2^{6-} fragment with a $Fe_3(CO)_9^{6+}$ fragment (filled through the t_{2g}-like set). The interactions of the $Fe_3(CO)_9$ fragment with the E_2 p_z symmetry-adapted linear combinations (SALCs) are described as σ-type and interactions involving the E_2 p_x and p_y symmetry-adapted linear combinations are described as π-type (Figure 1).

The description of bonding in many cluster systems is complex because the large number of energetically similar orbitals affords a large amount of mixing. A simplified description of the bonding follows. Filled−filled interactions between the P_2^{6-} fragment and the $Fe_3(CO)_9^{6+}$ t_{2g}-like set result in three sets of orbitals. Cluster orbitals 1a′ → 1a″ are primarily Fe_3-P_2 bonding, 2e′ and 2a′ are Fe_3-P_2 nonbonding, and orbitals 2e″ → 3e′ are $Fe_3(t_{2g}\text{-like})-P_2$ antibonding. There is little mixing of the e_g-like set into the lower energy cluster orbitals, but the third set of cluster orbitals is of appropriate energy to mix substantially with the $Fe_3(CO)_9$ e_g-like set. The normalized contributions of the t_{2g}-like, e_g-like, and E_2 fragment orbitals to the different sets of molecular orbitals are depicted in Figure 11 to illustrate this point. The $Fe_3(CO)_9$ e_g-like set of orbitals

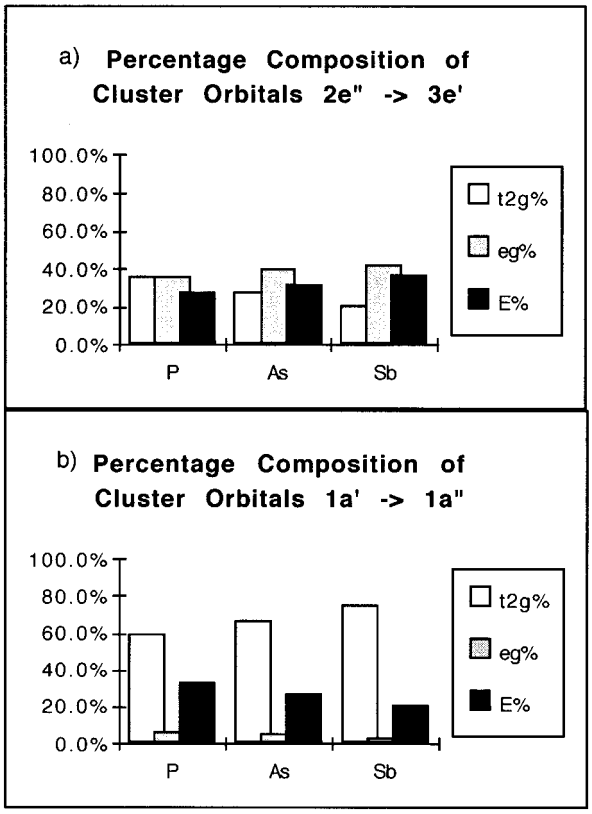

Figure 11. Normalized contributions of the $Fe_3(CO)_9$ t_{2g} and e_g and E_2 fragment orbitals are shown for the (a) 2e″, 3a′, 2a″, and 3e′ (2e″ → 3e′) and (b) 1a′, 1e′, 1e″, and 1a″ (1a′ → 1a″) sets of $Fe_3(CO)_9(\mu_3\text{-}E)_2$ cluster orbitals.

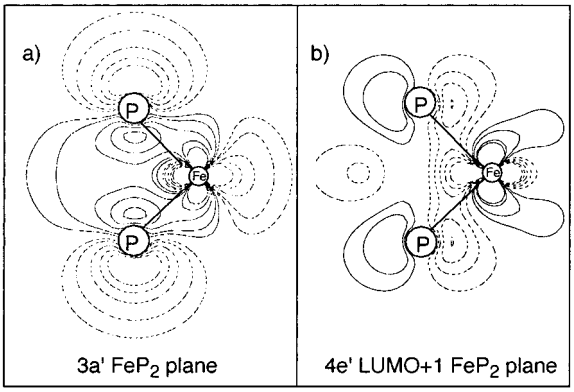

Figure 12. Contour plots of $Fe_3(CO)_9(\mu_3\text{-}P)_2$ orbitals showing representative metallophosphane orbitals with (a) lone pair character (3a′) and (b) π-accepting character (4e′). The contour plots are presented in the FeP_2 plane at levels of ±0.08, ±0.06, ±0.04, ±0.02, and ±0.01.

have greater radial extent and better directionality for Fe_3E_2 cluster bonding than the t_{2g}-like set; therefore, the 2e″ → 3e′ set of cluster orbitals is probably best described as slightly Fe_3E_2 bonding rather than nonbonding, although the degree of mixing ultimately determines the character of these orbitals.[29] The lowest unoccupied molecular orbital (LUMO), 4a′, is comprised solely of the $Fe_3(CO)_9$ 4a′ fragment because of the poor overlap with the a′ P_2 set that is directed at the center of the Fe_3 triangle. The LUMO and the next higher energy 4e′ set of cluster orbitals are strongly Fe−Fe antibonding. The 4e′ set of orbitals has a significant amount of P π-character (Figure 12).

(b) Cluster Bonding as a Function of E. The bonding description for clusters with capping As or Sb atoms is very

(27) For calculations on similar M_3E_2 systems, see: (a) Schilling, B. E. R.; Hoffmann, R. *J. Am. Chem. Soc.* **1979**, *101*, 3456−3467. (b) Rives, A. B.; Xiao-Zeng, Y.; Fenske, R. F. *Inorg. Chem.* **1982**, *21*, 2286−2294. (c) Evans, J. *J. Chem. Soc., Dalton Trans.* **1980**, 1005−1011. (d) North, T. E.; Thoden, J. B.; Spencer, B.; Dahl, L. F. *Organometallics* **1993**, *12*, 1299−1313. (e) van Hal, J. W.; Whitmire, K. H.; Zouchoune, B.; Halet, J.-F.; Saillard, J.-Y. *Inorg Chem.* **1995**, *34*, 5455−5460.

(28) (a) Hoffmann, R.; Albright, T. A.; Thorn, D. L. *Pure Appl. Chem.* **1978**, *50*, 1−9. (b) Elian, M.; Hoffmann, R. *Inorg. Chem.* **1975**, *14*, 1058−1076.

(29) Chesky, P. T.; Hall, M. B. *Inorg. Chem.* **1983**, *22*, 1339−1374.

Table 9. Mulliken Overlap Populations for the Uncapped Clusters $Fe_3(CO)_9(\mu_3\text{-}E)_2$, E = P, As, and Sb[a]

heteroatom	Fe_3-E_2 σ-overlap	Fe_3-E_2 π-overlap	Fe_3-E_2 total	Fe−Fe overlap
P	0.34_2	0.59_2	0.93_4	0.08_4
As	0.33_2	0.54_0	0.87_1	0.08_5
Sb	0.28_5	0.44_8	0.75_9	0.08_8

[a] The least significant digit is subscripted.

similar to that for $Fe_3(CO)_9(\mu_3\text{-}P)_2$. The variation in bonding as a function of heteroatom is primarily related to the fact that the E_2 orbital energies increase as P is substituted with As and then Sb, as expected on the basis of their relative electronegativities.[23] A secondary change is that the spread of energies for the $Fe_3(CO)_9$ fragment orbitals is smaller for the larger heteroatoms with longer Fe−Fe distances. The more electropositive heteroatoms interact less with the t_{2g}-like set and more with the e_g-like set because these E_2 fragment orbitals are higher in energy. Consequently, the 2e″ → 3e′ cluster orbitals have less of their E_2-e_g-like bonding character canceled out by E_2-t_{2g}-like antibonding character for larger E. There is greater heteroatom character in the lower energy cluster orbitals when E = P, and the cluster has greater $Fe_3(CO)_9$ e_g-like character when E = Sb (Figure 11).

Mulliken population analysis[30] confirms the qualitative analysis of the bonding trends. The E−Fe overlap populations are greatest when E = P (Table 9) as shown by the E_2−Fe_3 overlap populations (P, 0.93; As, 0.87; Sb, 0.76).[30b] Despite the range in average Fe−Fe distance of ∼0.14 Å, the Fe−Fe overlap populations are similar for all E (Fe−Fe overlap population: P, 0.08_4; As, 0.08_5; Sb, 0.08_8). The $Fe_3(CO)_9$ fragment orbitals that have the most Fe−Fe overlap are derived from the e_g-like set and participate in cluster bonding to the greatest degree when E = Sb. This observation is consistent with a recent *ab initio* analysis of the *closo*-borane clusters 1,5-$X_2B_3H_3$, where X = N, CH, P, SiH, and BH^-, by Schleyer and co-workers.[31] In this study they conclude that the degree of B−B interaction in the triboron core is *not* a function of B−B distance, but rather stronger B−B interactions are favored for the more electropositive caps.

(c) Metallopnictane Analogy. The description of the $Fe_3(CO)_9(\mu_3\text{-}E)_2$ clusters as metallopnictane ligands is supported by the $Fe_3(CO)_9(\mu_3\text{-}P)_2$ MO diagram. Similar to ER_3 groups, "lone pair" and "π-accepting" orbitals are observed. The energetically high-lying occupied 3a′ and 2a″ orbitals and the lower-lying 1a′ and 1a″ orbitals have substantial P lone pair character and are predisposed to interact in a σ-fashion with 16-electron ML_n fragments. Furthermore, the LUMO+1 orbitals (4e′) contain E π-character and are of the appropriate energy and symmetry to accept dπ electron density from a capping ML_n group (Figure 12). Calculations on the ML_n-capped clusters $Fe_3(CO)_9(\mu_3\text{-}EML_n)_2$ and subsequent Mulliken population analyses show the dominant interactions between the metallopnictane orbitals and the $(ML_n)_2$ fragment orbitals are described by a small set of orbitals. As illustrated in Figure 13, the "lone pair" orbitals of the metallophosphane $Fe_3(CO)_9(\mu_3\text{-}P)_2$ (1a′, 1a″, 3a′, and 2a″) are stabilized and the π-accepting 4e′ orbitals are destabilized upon interaction with the 16-electron metal fragments $[MnCp(CO)_2]_2$.

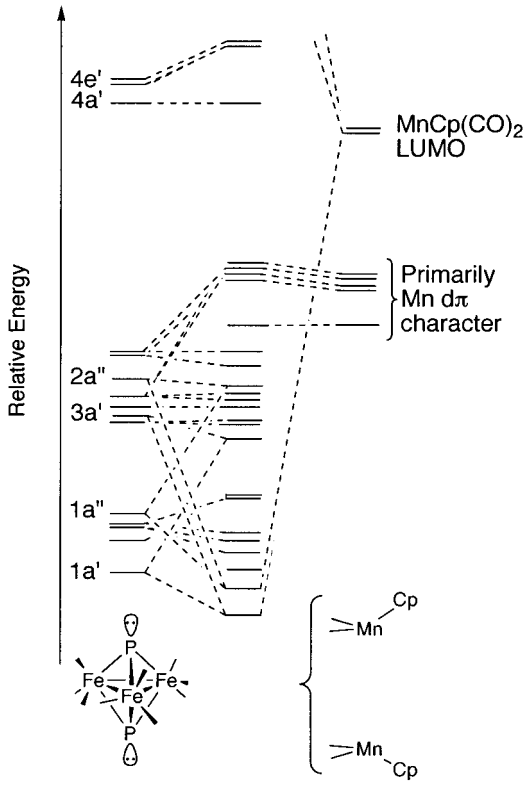

Figure 13. Frontier MO interactions between the metallophosphane $Fe_3(CO)_9(\mu_3\text{-}P)_2$ and the capping metal groups $[MnCp(CO)_2]_2$.

(d) M−E−M Angle. The consistency of the metallopnictane analogy suggests many of the trends in cluster bonding may be interpreted analagously to trends in organopnictane data. A Walsh correlation diagram analysis of ER_3 complexes that examines changes in orbital interactions as a function of R−E−R angle has provided a useful qualitative framework to explain experimental data.[32,33] Orpen and co-workers have examined an extensive body of data for 1292 $Z(PPh_3)$ complexes,[34] and a strong negative correlation between the P−C bond length and C−P−C bond angle in the $Z(PPh_3)$ complexes is observed. The Walsh analysis predicts that large C−P−C angles optimize the σ-donating properties of the PPh_3 ligand as well as the interactions between the phosphorus π-type orbitals (p_x and p_y) and the Ph_3 e′ SALC (Figure 1). Smaller C−P−C angles optimize the π-accepting properties of PPh_3 at the expense of the P−C bonding. The largest experimental bond angles are observed for σ-only acceptors such as a main-group elements while transition metal complexes, which act as σ-acceptors and π-donors, display C−P−C angles similar to those of PPh_3 due to counteracting effects. An analogous Walsh analysis of the bonding in the metallophosphane $Fe_3(CO)_9(\mu_3\text{-}P)_2$, in which the Fe−Fe distance is systematically increased while all other bond distances are held constant, is described below to probe changes in the interactions between the P_2 σ and π orbitals and the Fe_3 cluster face as a function of Fe−P−Fe angle. Extensions of this analysis to the interpretation of structural trends as a function of heteroatom are made.[17d]

As the Fe−P−Fe angle is increased by lengthening the Fe−Fe bonds, the Fe_3-P_2 σ-overlap population decreases while the

(30) a) Mulliken, R. S. *J. Chem. Phys.* **1955**, *23*, 1833−1846, 2338−2346. (b) The results of analyses comparing different atom pairs (E = P, As, Sb) should be done with caution due to the basis set dependence of the Mulliken population analysis. See: Levine, I. *Quantum Chemistry*, 4th ed.; Prentice Hall: Englewood Cliffs, NJ, 1991; pp 475−478.

(31) Schleyer, P. R.; Subramanian, G.; Dransfeld, A. *J. Am. Chem. Soc.* **1996**, *118*, 9988−9989.

(32) Walsh, A. D. *J. Chem. Soc.* **1953**, 2260−2306.

(33) (a) Albright, T. A.; Burdett, J. K.; Whangbo, M.-H. *Orbital Interactions in Chemistry*; Wiley: New York, 1985. (b) Gimarc, B. M. *Molecular Structure and Bonding*; Academic Press: New York, 1979. (c) Reference 17. (d) Reference 36.

(34) Dunne, B. J.; Morris, R. B.; Orpen, A. G. *J. Chem. Soc., Dalton Trans.* **1991**, 653−661.

Table 10. Mulliken Population Analysis for $Fe_3(CO)_9(\mu_3\text{-}P)_2$[a,b]

Fe−Fe dist (Å)	Fe−E−Fe (deg)	E_2-Fe_3 σ-overlap[c]	E_2-Fe_3 π-overlap[c]	E_2-Fe_3 total overlap	Fe−Fe total overlap	E−E overlap	E_2 Mulliken charge	Fe_3 Mulliken charge
2.536	67.9	0.34_8	0.56_3	0.91_1	0.10_6	-0.01_9	−0.63	0.22
2.636	71.0	0.34_2	0.60_2	0.94_4	0.08_1	-0.01_9	−0.72	0.30
2.736	74.1	0.33_0	0.64_0	0.96_9	0.05_6	-0.01_8	−0.81	0.38
2.836	77.3	0.30_8	0.67_8	0.98_7	0.03_2	-0.01_5	−0.89	0.45
2.936	80.5	0.27_6	0.71_8	0.99_4	0.00_8	-0.00_9	−0.95	0.51
2.986	82.2	0.25_5	0.73_8	0.99_3	-0.00_0	-0.00_3	−0.97	0.52

[a] All interatomic distances are kept constant except for Fe−Fe and E···E distances (Fe−P = 2.260 Å). [b] The least significant digit is subscripted. [c] The σ and π designators refer to the a_1 (E s,p_z) and e (E p_x,p_y) sets of orbitals, respectively.

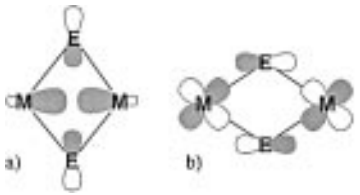

Figure 14. Representative (a) σ-type and (b) π-type orbital interactions for a dinuclear M_2-E_2 system. The M−E−M angles chosen for (a) and (b) reflect the optimal overlap for each type of interaction.

π-overlap population increases (Table 10). A representation of the relevant orbital interactions that give rise to this trend for the simple example of a dinuclear complex is depicted in Figure 14. The Mulliken charge for P also increases as the angle is increased, suggesting that larger Fe−E−Fe angles should be favored for the more electronegative E groups. Predictions based on this Walsh analysis are borne out in calculations for the $Fe_3(CO)_9(\mu_3\text{-}E)_2$ clusters. The ratio of Fe_3-E_2 π-bonding to Fe_3-E_2 σ-bonding changes as a function of E (Table 9), and the π to σ ratio is largest for the phosphorus-capped cluster, the cluster with the largest average Fe−E−Fe bond angle and the largest Fe_3-E_2 overlap population.[30b] These trends are consistent with an analysis of the bonding in $Ni_3Cp'_3(\mu_3\text{-}CS)(\mu_3\text{-}CO)$ presented by Dahl and co-workers.[35] The authors rationalize that the Ni−CS distance (1.92 Å) in the cluster $Ni_3Cp'_3(\mu_3\text{-}CS)(\mu_3\text{-}CO)$ is shorter than the Ni−CO distance (1.95 Å) because the thiocarbonyl ligand is a better π-acceptor with respect to the $Ni_3(Cp')_3$ cluster face than the carbonyl ligand. The shorter Ni−CS distance requires that the $Ni-C_S-Ni$ angle (77.0°) be larger than the $Ni-C_O-Ni$ angle (75.6°). Similar to Dahl's conclusions concerning the role of the bridging heteroatoms in establishing M_2E_2 dimer geometry,[1a] we conclude that larger M−E−M angles in the metallopnictane ligands are favored for more electronegative E.

The Fe−Fe overlap populations decrease with increasing Fe−Fe bond length in the $Fe_3(CO)_9(\mu_3\text{-}P)_2$ calculations. In calculations for the $Fe_3(CO)_9(\mu_3\text{-}E)_2$ clusters presented above, the Fe−Fe overlap populations are nearly constant as the Fe−Fe bond distance increases to accommodate the larger heteroatoms. These two results together support the idea that the degree of Fe−Fe interaction in these clusters is dictated by the electronic characteristics of the capping E (or EML_n) groups.

Further Comments on the Metallopnictane. The isolation and characterization of $(\mathbf{1\text{-}P})^{2-}$ enables characterization of the electronic impact of the dinegatively-charged metallophosphane ligand, $[Fe_3(CO)_9(\mu_3\text{-}P)_2]^{2-}$. The infrared CO stretching modes attributable to $MnCp(CO)_2$ overlap with the Fe_3-core CO bands in the infrared spectrum of $(\mathbf{1\text{-}P})^{2-}$; therefore, the structural data are the only tools available to analyze the donor properties of the metallopnictane ligands. The average P−Mn distance in $(\mathbf{1\text{-}P})^{2-}$ of 2.252(5) Å is elongated by 0.11 Å over the average Mn−P distance in the 48-electron cluster **1-P**. The lengthened Mn−P distances in $(\mathbf{1\text{-}P})^{2-}$ are comparable to that in $MnCp(CO)_2(PPh_3)$ (Table 4). The metallophosphane analogy provides a simple explanation for these data. Reduction of the cluster and the subsequent localized Fe−Fe bond cleavage[4] results in occupation of one of the orbitals which was shown to be a π-accepting orbital for the neutral metallopnictane $Fe_3(CO)_9(\mu_3\text{-}E)_2$ (Figure 11). Partial occupancy of this orbital in $Fe_3(CO)_9(\mu_3\text{-}P)_2^{2-}$ reduces the multiple bond character of the Mn−P bond, resulting in an increased P−Mn distance in $(\mathbf{1\text{-}P})^{2-}$. This orbital explanation is not the only way to justify the increased P−Mn distance in the dianion, but the orbital description is simple and consistent.

Table 11. Interatomic Distances Used in Fenske−Hall MO Calculations

heteroatom	Fe−Fe (Å)	Fe−E (Å)	Fe−C (Å)	C−O (Å)
P	2.623	2.271	1.80	1.14
As	2.690	2.360	1.80	1.14
Sb	2.768	2.531	1.80	1.14

The π-back-bonding interaction between manganese and the metallophosphane ligand is diminished by the two-electron reduction of the metallophosphane ligand. Orpen and Connelly demonstrated that a similar change in $M-ER_3$ bond distance is observed upon oxidation of the coordinated metal.[36] For example, the average M−P bond distance in $CpCo(PEt_3)_2$ (2.218(1) Å) increases by 0.08 Å upon oxidation of the metal due to loss of M dπ-t*o*-PR_3 donation.[37] The P−R σ* nature of π-acceptor orbitals in the PR_3 ligands is also supported by shorter P−R distance in $CpCo(PEt_3)_2^+$. In the metallopnictane complexes, the $E-ML_n$ bond distance would presumably be affected similarly by oxidation of the capping metal complex or by reduction of the metallopnictane ligand.

Conclusions. The synthesis of a series of $Fe_3(CO)_9(\mu_3\text{-}EML_n)_2$ clusters that differ by either a capping heteroatom and/or a capping metal group has allowed a systematic investigation of the cluster properties. The electronic characteristics of the capping ML_n groups directly influence the electron density at the Fe_3 core. Clusters with electron-rich ML_n groups are reduced at more negative potentials, and the Fe_3-core CO stretching frequencies are observed at lower energy. The changes in capping heteroatom also influence electron density at the Fe_3 core, but the structural change attendant upon incorporating a larger heteroatom, together with the resultant lowering of the LUMO energy, is the dominant factor in determining the trend in reduction potentials. Studies of the structures and bonding in organopnictane complexes provide a framework for interpretation of the structural data and bonding in the $Fe_3(CO)_9(\mu_3\text{-}EML_n)_2$ clusters. The metallopnictane ligand

(35) North, T. E.; Thoden, J. B.; Spencer, B.; Bjarnason, A.; Dahl, L. F. *Organometallics* **1992**, *11*, 4326−4337.

(36) Orpen, A. G.; Connelly, N. G. *J. Chem. Soc., Chem. Commun.* **1985**, 1310−1311. Orpen, A. G.; Connelly, N. G. *Organometallics* **1990**, *9*, 1206−1210.

(37) Harlow, R. L.; McKinney, R. J.; Whitney, J. F. *Organometallics* **1983**, *2*, 1839−1842.

Table 12. Crystallographic Experiments and Computations for $Fe_3(CO)_9[\mu_3\text{-}AsMnCp(CO)_2]_2$ (**1-As**), $Fe_3(CO)_9[\mu_3\text{-}SbMnCp(CO)_2]_2$ (**1-Sb**), $Fe_3(CO)_9[\mu_3\text{-}PCr(CO)_5]_2$ (**2-P**), $Fe_3(CO)_9[\mu_3\text{-}AsCr(CO)_5]_2$ (**2-As**), $Fe_3(CO)_9[\mu_3\text{-}SbCr(CO)_5]_2$ (**2-Sb**), and $[(CH_2C_6H_5)(CH_3)_3N]_2\{Fe_3(CO)_9[\mu_3\text{-}PMn(C_5H_5)(CO)_2]_2\}$ (**1-P**)$^{2-}$

	1-As	**1-Sb**	**2-P**	**2-As**	**2-Sb**	$[(PhCH_2)Me_3N]_2$(**1-P**)
formula	$C_{23}H_{10}As_2Fe_3Mn_2O_{13}$	$C_{23}H_{10}Sb_2Fe_3Mn_2O_{13}$	$C_{19}Cr_2Fe_3O_{19}P_2$	$C_{19}As_2Cr_2Fe_3O_{19}$	$C_{19}Sb_2Cr_2Fe_3O_{19}$	$C_{43}H_{42}Fe_3O_{13}P_2Mn_2$
fw	921.57	1015.23	865.67	953.56	1047.22	1134.17
temp, K	298	103	298	298	298	298
space group	$P2_1/c$	$P2_1/c$	$P\bar{1}$	$P\bar{1}$	$P\bar{1}$	Cc
a, Å	15.6964(14)	17.584(3)	8.978(3)	9.0047(13)	9.1049(12)	21.417(4)
b, Å	8.5234(12)	10.9043(9)	9.826(3)	10.0693(9)	10.4578(14)	12.6755(19)
c, Å	22.072(3)	15.592(3)	99.70(3)	16.7760(23)	16.2520(13)	19.231(4)
α, deg	90	90	96.16(3)	81.948(9)	81.519(9)	90
β, deg	92.941(9)	107.166(17)	97.65(3)	76.882(12)	83.296(9)	116.55(2)
γ, deg	90	90	99.70(3)	82.920(9)	80.129(11)	90
V, Å^3	2949.0(7)	2856.6(8)	1419.1(8)	1460.2(3)	1500.3(3)	4670(2)
Z	4	4	2	2	2	4
F(000)	1791.07	1928.48	847.8	919.56	988.27	2311.73
λ(Mo Kα), Å	0.7093	0.7093	0.7093	0.7093	0.7093	0.7093
μ(Mo Kα), cm^{-1}	45.3	42.4	24.2	44.9	39.6	15.5
d_{calc}, g cm^{-3}	2.076	2.361	2.026	2.169	2.318	1.613
R^a	0.044	0.047	0.068	0.042	0.045	0.063
$R_w{}^b$	0.049	0.068	0.069	0.05	0.056	0.058

^{a} $R = (\sum||F_o| - |F_c||)/\sum|F_o|$. ^{b} $R_w = [\sum w(|F_o| - |F_c|)^2/\sum w(F_o)^2]^{1/2}$.

description of the $Fe_3(CO)_9(\mu_3\text{-}E)_2$ cluster is shown to be both chemically and theoretically relevant. The E−ML_n interaction can be tuned in metallopnictane complexes by a two-electron reduction at the Fe_3 core, which diminishes the acceptor properties of the metallopnictane ligand. This ability to use redox chemistry to modulate the donor properties of metallopnictane ligands is a feature that distinguishes them from organopnictane ligands.

Experimental Section

Materials and General Procedures. All manipulations were carried out under nitrogen using standard Schlenk techniques. Tetrahydrofuran (THF), pentane, and toluene were freshly distilled from sodium benzophenone ketyl. Dichloromethane was freshly distilled from P_4O_{10}. Chromatography was performed at room temperature, florisil (Fisher Scientific, 100−200 mesh) was used as a support, and chromatography solvents were degassed. Phosphorus trichloride (Johnson Matthey Electronics) was degassed and vapor distilled, and antimony trichloride (Strem) was sublimed before use. Hexacarbonylchromium (Strem), cyclopentadienylmanganese tricarbonyl (Strem), diiron nonacarbonyl (Strem), and arsenic trichloride (Strem 99.99% pure) were used as received. Disodium octacarbonylferrate, disodium tetracarbonylferrate,[38] $(Cl_3P)Cr(CO)_5$,[39] $ClSb[MnCp(CO)_2]_2$,[40] and the clusters **1-P**, **2-As**, and **2-Sb**[6] were prepared by literature procedures. Photolysis reactions were performed with a Hanova lamp (UV 450 W) at 10 °C.

Spectroscopic Measurements. Proton NMR spectra were recorded on a Bruker ACX-250 machine and referenced to $CHCl_3$. Phosphorus spectra were recorded on a Bruker AC-250 spectrophotometer operating at 121.50 MHz and referenced to solvent. IR spectra were recorded on a Bomem Michelson 120 spectrometer. Mass spectra were collected by Asoka Ranasinghe (UNC-CH Environmental Science and Engineering). Mass spectra were obtained with a VG 70-250 SEQ instrument by electron impact at 35 eV. The sample was introduced by a solid probe, and no heating was necessary (ion source temperature ∼250 °C).

Electrochemical Measurements. Electrochemical experiments were performed with a Princeton Applied Research Model 273 potentiostat/galvanostat equipped with a Yokogawa 3025 X-Y recorder. Cyclic voltammograms were observed in a single-compartment airtight three-electrode cell under nitrogen using positive feedback *iR* compensation. A glassy carbon working electrode and a Pt-wire counter electrode were employed. The potential was referenced to a Ag/0.1 M $AgNO_3$ (CH_3CN solution) reference electrode, which was separated from the analyte solution by placement in a vycor-glass-tipped compartment. For comparison of the different clusters each sample contained ferrocene, and the Cp_2Fe^+/Cp_2Fe couple was used as an internal standard. The cyclic voltammograms were performed in 0.1 M solution of $(n\text{-}Bu_4N)(BF_4)$ in CH_2Cl_2 or CH_3CN. Spectroelectrochemical experiments were performed in a specially equipped transparent IR cell.

Fenske−Hall Calculations. Calculations were performed using the Fenske−Hall method,[26] the results of which depend only on the internal geometry and choice of basis functions. The geometry was optimized to C_{3h} symmetry for the $Fe_3(CO)_9$. The cluster geometries were constructed based on average interatomic distances and angles for the crystal structures, but the Fe−C and C−O bond distances were kept constant with changes in E (Table 11). The Walsh analysis was performed keeping all of the bond lengths in the $Fe_3(CO)_9(\mu_3\text{-}P)_2$ model constant except the Fe−Fe distances which were increased stepwise to 2.986 Å. The basis sets were generated previously[41] by a best fit to Herman−Skillman atomic calculations[42] using the method of Bursten, Jensen, and Fenske.[43]

Preparation of $Fe_3(CO)_9[\mu_3\text{-}AsMnCp(CO)_2]_2$ (1-As). A sample of $MnCp(CO)_3$ (555 mg, 2.9 mmol) was dissolved in 100 mL of THF and photolyzed for 30 min. An equimolar amount of $AsCl_3$ was added by microliter syringe at 0 °C, and the solution was allowed to warm to room temperature. The reaction was monitored by IR until the $MnCp(CO)_2(THF)$ peaks disappeared. The solvent was removed under vacuum, and the dark purple residue was extracted with 25 mL of pentane, filtered, and cannulated into a toluene (60 mL) suspension of $Fe_2(CO)_9$ (5.0 g, 13.7 mmol). The reaction mixture was heated at 45−50 °C for ∼6 h. The solvent was removed, and column chromatography on a florisil support was performed. A green band identified as $Fe_3(CO)_{12}$ eluted with hexanes. A reddish band identified as $Fe_4(CO)_{14}(\mu_4\text{-}AsCl)$ by IR and mass spectrometry was eluted with hexanes/toluene (8/1).[44] **1-As** was collected as a reddish-purple band with hexanes/toluene (3/1) and was recrystallized from dichloromethane/pentane. Yield: 25 mg, 0.03 mmol, 2% based on $MnCp(CO)_3$. The mass spectrum displayed a peak attributable to the parent ion *m/e* 921 and peaks corresponding to the loss 13 CO ligands.

Preparation of $Fe_3(CO)_9[\mu_3\text{-}SbMnCp(CO)_2]_2$ (1-Sb). A sample of $ClSb[MnCp(CO)_2]_2$ (530 mg, 1.0 mmol) in toluene was reacted with

(38) Strong, H.; Krusic, P. J.; San Filippo, J.; Keenan, S.; Finke, R. G. *Inorg. Synth.* **1986**, *24*, 157−161.
(39) Lang, H.; Zsolnai, L.; Huttner, G. *Z. Naturforsh* **1985**, *40b*, 500−506.
(40) Weber, U.; Zsolnai, L.; Huttner, G. *J. Organomet. Chem.* **1984**, *260*, 281−291.
(41) Harris, S. *Organometallics* **1994**, *13*, 2628−2640.
(42) Herman, F.; Skillman, S. *Atomic Structure Calculations*; Prentice-Hall; Englewood Cliffs, NJ, 1963.
(43) Bursten, B. E.; Jensen, J. R.; Fenske, R. F. *J. Chem. Phys.* **1978**, *68*, 3320−3321.
(44) Zimler, T.; Vizi-Orosz, A.; Marko, L. *Transition Met. Chem.* **1977**, *2*, 97−99.

$Na_2Fe_2(CO)_8$ (400 mg, 1.1 mmol). The reaction was allowed to stir at room temperature for 2.5 h. The solvent was removed, and **1-Sb** was isolated in a manner similar to that for **1-As**. Several attempts were made to reproduce this synthesis so further studies and characterizations could be made. All attempts however failed. Yield: 5 mg, 5 μmol, 0.5% based on $ClSb[MnCp(CO)_2]_2$.

Preparation of $Fe_3(CO)_9[\mu_3\text{-}PCr(CO)_5]_2$ (2-P). To a suspension of $Fe_2(CO)_9$ (3.5 g, 9.6 mmol) in toluene was added a toluene solution of $(Cl_3P)Cr(CO)_5$ (0.50 g, 1.5 mmol). The suspension was heated under static vacuum at 70 °C for 6 h. The solution turned deep maroon upon heating. The solvent was removed under vacuum. Workup is analogous to **1-As** except the asymmetric cluster $Fe_3(CO)_9[\mu_3\text{-}PCr(CO)_5][\mu_3\text{-}PFe(CO)_4]$ (**4-P**)[6] was eluted with hexanes/toluene (8/1) and **2-P** was eluted with hexanes/toluene 3/1. The two clusters were difficult to separate completely from one another, but **2-P** was successfully isolated by fractional recrystallization as **4-P** is more soluble in pentane than is **2-P**. Yield: **2-P**, 82 mg, 0.09 mmol, 11% based on $(Cl_3P)Cr(CO)_5$; **4-P**, 10 mg, 0.01 mmol, 1% based on $(Cl_3P)Cr(CO)_5$. NMR spectrum for **2-P**: $\delta(^{31}P)$ 764.9 (s). The mass spectrum displayed a peak attributable to the parent ion *m/e* 866 and peaks corresponding to the loss of 17 CO ligands.

Preparation of $[(PhCH_2)Me_3N]\{Fe_3(CO)_9[\mu_3\text{-}PMnCp(CO)_2]_2\}$. The salt $[(PhCH_2)Me_3N]_2$(**1-P**) was prepared by an analogous procedure to the $(Ph_3P)_2N^+$ salt.[4] Following the Na/Ph_2CO reduction of **1-P**, a metathesis reaction was carried out by addition of a MeOH solution of 2 equiv of $[(PhCH_2)Me_3N]Cl$. After the solution was stirred for 1 h, the solvent was removed under vacuum. The residue was dissolved in THF, the resulting solution was filtered, and crystals of $[(PhCH_2)Me_3N]_2$(**1-P**) were obtained by layering the THF solution with *i*-Pr_2O.

X-ray Structure Determinations. Crystallographic data and experimental parameters are available in Table 12 and as Supporting Information. The structures were solved using software from the NRCVAX computing package.[45] Least-squares refinement on *F* minimized the function $\sum(|F_o| - |F_c|)^2$. Crystals were grown either by slow diffusion of pentane into a CH_2Cl_2 solution of the cluster or by the slow evaporation of the solvent over a period of days from a CH_2Cl_2 solution of the cluster. The Fe_3 cluster in **1-As** was oriented in two different positions in the crystalline lattice related by a rotation about the As−As axis. After initial structure solution, three peaks were located in the difference map and assigned as a rotated Fe_3 triangle with 8.5% occupancy. The crystals of **2-P** were of relatively poor quality, and attempts to grow better quality crystals failed. Due to limited number of observable reflections, only the Fe, P, and Cr atoms were refined anisotropically.

Acknowledgment. B.E.C. thanks Dr. Suzanne Harris (U. of Wyoming) for helpful discussions and insight into interpreting bonding data and Michael Palmer (U. of Wyoming) for help in obtaining and running the Fenske−Hall program and supporting computer programs. Partial support for this research was provided by the Department of Education (Graduate Assistant in Areas of National Need fellowship to B.E.C.) and the National Science Foundation (Grant CHEM-9626156).

Supporting Information Available: Infrared spectra of the CO stretching region for **1-P** and partially enriched ^{13}CO **1-P** and those taken during the electrochemical reduction of **2-As** (2 pages). X-ray crystallographic files, in CIF format, for complexes **1-As**, **1-Sb**, **2-P**, **2-As**, **2-Sb**, and $(\mathbf{1\text{-}P})^{2-}$ are available on the Internet only. Ordering and access information is given on any current masthead page.

IC970786A

(45) Gabe, E. J.; Le Page, Y.; Charland, J.-P.; Lee, F. L.; White, P. S. *J. Appl. Crystallogr.* **1989**, *22*, 384−387.